J Fluoresc (2011) 21:393–407
DOI 10.1007/s10895-010-0728-8

ORIGINAL PAPER

Two-Photon Optical Properties of Novel Branched Conjugated Derivatives Carrying Benzophenone Moiety with Various Electron Donor-Acceptor Substituent Groups

Hongru Li · Long Yang · Jian Liu · Chunfeng Wang · Fang Gao · Shengtao Zhang

Received: 12 June 2010 / Accepted: 8 September 2010 / Published online: 1 October 2010

Abstract This paper presents a range of novel new branched conjugated dyes containing benzophenone moiety. As compared with those of 4-(*p*-benzoyl-styrene)yl-4′-(styrene)yl-triphenylamine (**C1**) and 4-(*p*-benzoyl-styrene) yl-4′-3,4,5-trimethoxyl-styrene)yl-triphenylamine (**C2**), the maximal linear absorption and emission wavelength of 4-(*p*-benzoyl-styrene)yl-4′-(*p*′-nitro-styrene)yl-triphenylamine (**C3**) displays red-shifted remarkably, While the fluorescence quantum yields of **C3** are lower than those of **C1** and **C2** in various solvents. The fluorescence lifetimes of the derivatives were measured, and radiative and non-radiative transition constants of the derivatives were calculated. Two-photon absorption (TPA) optical data of the derivatives were measured by Ti:sapphire femtosecond laser tuning from 720 to 880 nm at intervals of 20 nm. TPA induced fluorescence emission of **C3** is red-shifted with respected to that of **C1** and **C2**. TPA cross sections of **C3** are larger than those of **C1** and **C2** in various excited laser frequencies. TPA cross section of **C2** and **C3** are much larger than those of 3,4,5-(trimethoxylstyrene)yl-triphenylamine (**C4**) and 4-(*p*-nitrostyrene)yl-triphenylamine (**C5**) respectively under various near-IR Ti:sapphire femtosecond laser wavelength. **C1** and **C2** show similar one- and two- photon optical nature. Geometry optimization with ab initio method confirms that **C3** has different electron density distribution, the energy levels in frontier orbitals, the dipole moment changes, the absorption and emission spectroscopy from those of **C1** and **C2**. The cyclic voltammograms of the derivatives were detected in methylene chloride at various scan rates, and the energy of frontier orbials were estimated further from the redox potentials.

Keywords Optical properties · Conjugated derivative · Benzophenone moiety · Subsitutent group effect · Cyclic voltammograms

H. Li (✉) · L. Yang · J. Liu · C. Wang · F. Gao (✉) · S. Zhang
College of Chemistry and Chemical Engineering,
Chongqing University,
Chongqing 400044, China
e-mail: hongrli1972@gmail.com

F. Gao
e-mail: fanggao1971@gmail.com

Introduction

The application potentials of highly fluorescent and two-photon absorption dyes in a wide range of fields, such as two-photon fluorescence sensors [1–3], two-photon fluorescence excitation microscopy [4–7], three-dimensional optical data storage and microfabrication [8, 9], optical limiting materials [10, 11], and two-photon photodynamic therapy [12–14], has stimulated the survey of new conjugated dyes. In looking for high quality organic dyes with ideal optical nature, the chemical structures of the dyes have been shown to a strong relationship with the optical characteristics. Consequently, the investigation of the relationship between molecular structure and optical properties of two-photon dyes receives considerable attention. Since Marder and coauthors have discovered that some bis(styryl)benzene derivatives with D-π-D, D-π-A and D-A-D structural motifs showed excellent two-photon optical properties [15, 16], a substantial number of scientists have explored the investigation of such derivatives [17–22], and two factors was found to play crucial role on the regulation of the optical properties: (1) the

conjugated length of the molecules, which could be increased by the insertion of phenylene-vinylene or phenylene-butadienylene groups. (2) the extent of the symmetrical charge transfer from the ends of the molecules to the middle, or vice versa. This indicates that the electron density distribution of frontier orbitals of the derivatives could be mediated well via the enhancement of number of branches and the variation of substituent groups, and thus the optical character could be regulated. Although some endeavors have been made to investigate the optical properties of conjugated triphenylamine-cored derivatives containing electron-donating substituent groups [22, 23], while the comparable studies on the optical properties of such derivatives bearing with various electron-donating and electron-withdrawing groups are seldomly reported.

Benzophenone is a well-known photoactive compound and is used extensively in material and biomedical fields [24, 25]. We could imagine that if a two-photon chromophore is linked with benzophenone via conjugated double bond, the new derivatives have great application potentials in various fields. Furthermore, benzophenone unit could play acceptor-donor role because of electron-withdrawing effect of carbonyl group. Herein, we employed various push-pull substituent groups, including nitro and methoxy groups, to tune the electron density distribution of the frontier orbitals of branched conjugated derivatives containing benzophenone moiety with the purpose to reveal the effect of the substituent group on one- and two- photon optical properties of the derivatives. We describe new branched conjugated derivatives carrying benzophenone part, including 4-(*p*-benzoylstyrene) yl-4′-(styrene)yl-triphenylamine (**C1**), 4-(*p*-benzoylstyrene) yl-4′-3,4,5-trimethoxylstyrene)yl-triphenylamine (**C2**), 4-(*p*-benzoyl styrene)yl-4′-(*p*′-nitrostyrene)yl-triphenylamine (**C3**) in this paper. As shown in Fig. 1, the substituent group is in one branch, and benzophenone part locates at the other branch. Each branch forms a π conjugated structure and the overall conjugation of the derivatives are efficiently extended. So, two-photon absorption nature could be enhanced, and the effect of substituent group on the optical properties of such derivatives could be observed. In order to confirm the effect of benzopheonone branch on the TPA nature of the derivatives, we further compared TPA properties of **C2** and **C3** with those of 3,4,5-trimethoxylstyrene)yl-triphenylamine (**C4**), 4-(*p*-nitrostyrene)yl-triphenylamine (**C5**) in this manuscript. We also determined the fluorescence lifetime and the cyclic voltammograms of the derivatives, and performed

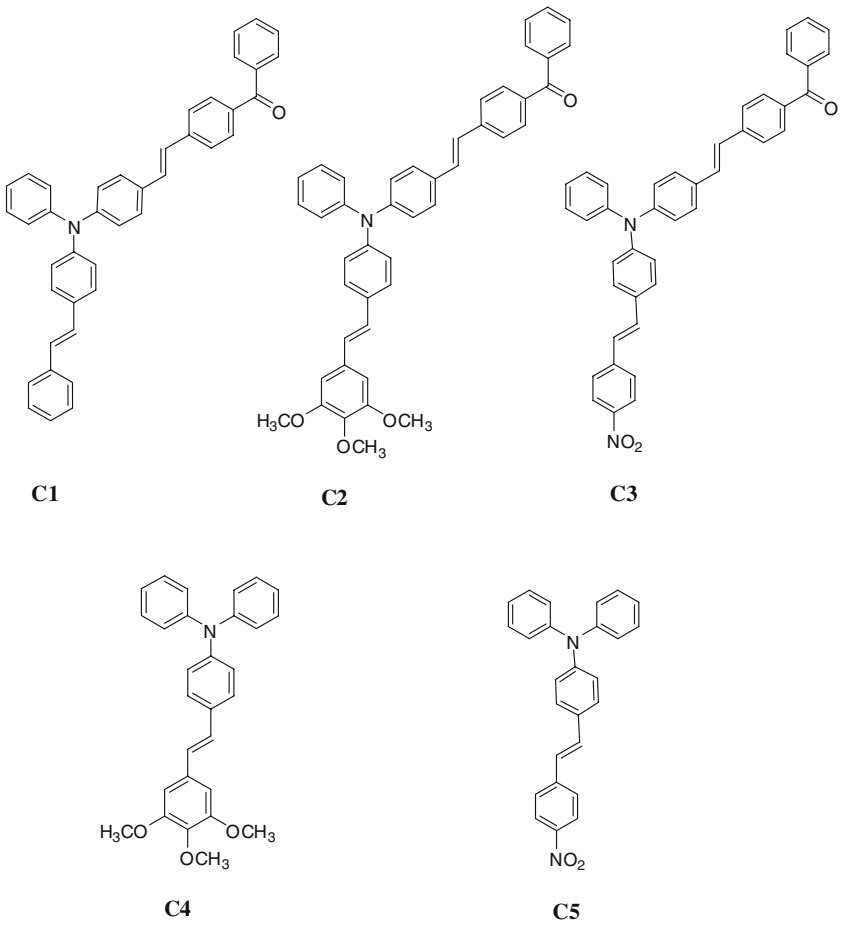

Fig. 1 Chemical structures of **C1**, **C2** and **C3**

molecular geometry optimization calculations to understand deeply the interrelationship between the chemical structures and the optical characteristics,

Experimental

Reagents and Materials

Organic solvents were obtained from Chongqing Medical and Chemical Corporation. Other chemicals and reagents were purchased from Aldrich unless otherwise specified. The organic solvents were dried using standard laboratory techniques according to well-known methods [26]. The starting materials were further purified with redistillation or recrystallization before use. **C1** to **C3** (Fig. 1) were prepared in our laboratory. Synthesis of reference TPA compounds **C4** and **C5** will be reported elsewhere [27].

One- and Two-Photon Optical Measurement and Structural Characterization

The UV/visible absorption spectra (1×10^{-5} mol/L) were recorded with a Cintra spectrophotometer. The emission spectra (1×10^{-6} mol/L) were checked with Shimadzu RF-531PC spectrofluorophotonmeter. Rodamin 6G in ethanol (Φ=0.94, 1×10^{-6}–1×10^{-5} mol/L [28]) was used as reference to determine the fluorescence quantum yields of the compounds herein. To avoid self-quenching of fluorescence emission, low concentration of the compounds (1×10^{-6} mol/L) was prepared for the survey of fluorescence quantum yields. The melting point was determined using a Beijing Fukai melting point apparatus. Nuclear magnetic resonance (NMR) spectroscopy was conducted at room temperature on a Bruker 500 MHz apparatus with tetramethylsilane (TMS) as an internal standard and $CDCl_3$ as solvent. Elemental analysis was performed by a CE440 elemental analysis meter from Exeter Analytical Inc. FT-IR spectra were recorded on a Nicolet Magna-IR 550-II in the region of 4,000–400 cm^{-1} using KBr pellets spectrophotometer.

The fluorescence quantum yields of the compounds in solvents with different polarities were measured based on the following equation [29, 30]:

$$\Phi_{\mathrm{f}} = \Phi_{\mathrm{f}}^{0}\frac{n_0^2 A^0 \int I_{\mathrm{f}}(\lambda_{\mathrm{f}})\mathrm{d}\lambda_{\mathrm{f}}}{n^2 A \int I_{\mathrm{f}}^{0}(\lambda_{\mathrm{f}})\mathrm{d}\lambda_{\mathrm{f}}} \tag{1}$$

wherein $\boldsymbol{n_0}$ and $\boldsymbol{n}$ are the refractive indices of the solvents, $\boldsymbol{A^0}$ and $\boldsymbol{A}$ are the optical densities at excitation wavelength, $\boldsymbol{\Phi_f}$ and $\boldsymbol{\Phi_f^0}$ are the quantum yields, and the integrals denote the area of the fluorescence bands for the reference and sample, respectively.

Two-photon excited fluorescence spectra, pumped by Ti: sapphire femto-second laser (Spectra-Physics Ltd., Tsunami mode-locked, 80 MHz, <130 f s, average power ≤700 mW) tuned by step of 20 nm in the range of 700~880 nm, were recorded on Ocean Optics USB2000 CCD camera with detecting range of 180~880 nm. Two-photon absorption (TPA) cross-section (σ) was determined by up-conversion fluorescence method using 5×10^{-4} mol/L fluorescein in 0.1 mol/L solution of NaOH as reference sample [31]. The sample was bubbled with N_2 for 15 min to eliminate O_2 before the detection. Two-photon absorption crossing sections of the compounds were determined by the following equations [31, 32]:

$$\sigma = \frac{\sigma^{TPE}}{\Phi_F} \tag{2}$$

$$\sigma^{TPE} = \sigma_{cal}^{TPE}\frac{c_{cal}}{c}\frac{n_{cal}}{n}\frac{S}{S_{cal}} \tag{3}$$

Wherein $\boldsymbol{\sigma}$ is two-photon absorption section, $\boldsymbol{\sigma^{TPE}}$ represents as two-photon excited crossing section, $\boldsymbol{c}$ is concentration of reference and sample molecules, n shows refractive index of the solvent, and $\boldsymbol{S}$ is two-photon up-conversion fluorescence intensity, ***cal*** denotes as reference.

In order to eliminate saturation photophysical processes and ensure the two-photon excited fluorescence intensity being quadratically dependent on excitation intensity, the excitation powers in our TPA cross-section measurements were limited below 130 mW.

One-Photon Fluorescence Lifetimes

One-photon fluorescence lifetimes of the derivatives were determined using a Horiba NAES-1100 time-corrected single photon counting unit. Lifetimes were calculated from the decay curves using a least-square method.

Molecular Geometry Optimization

The calculations were performed by means of the Gaussian 03 program package. The geometry optimization of enol and keto forms for the ground electronic state (S_0) was carried out with HF (Hartree-Fock) method using the B3LYP method both [33–35], while the CIS (Configuration Interaction Singles-excitation) has been employed to optimize the geometries of the first singlet excited state (S_1) of the derivatives. Although the CIS method has been shown to produce basically reliable geometries and force-fields, it predicts much too high excitation energies (by *ca*. 1 eV) [33]. To correct the errors and introduce the dynamic

electron correlation, TDDFT (time-dependent DFT) was performed to predict energies at the HF and CIS optimized geometries for S_0 and S_1 state respectively, namely TDDFT//HF or TDDFT//CIS (denoted as single-point calculation//optimization method) [36], the latter was used to analyze the fluorescence properties of the derivatives in the excited state. While the TDDFT//HF and was used for the calculation of absorption spectra.

Scheme 1 Synthesis of **C1**, **C2** and **C3**

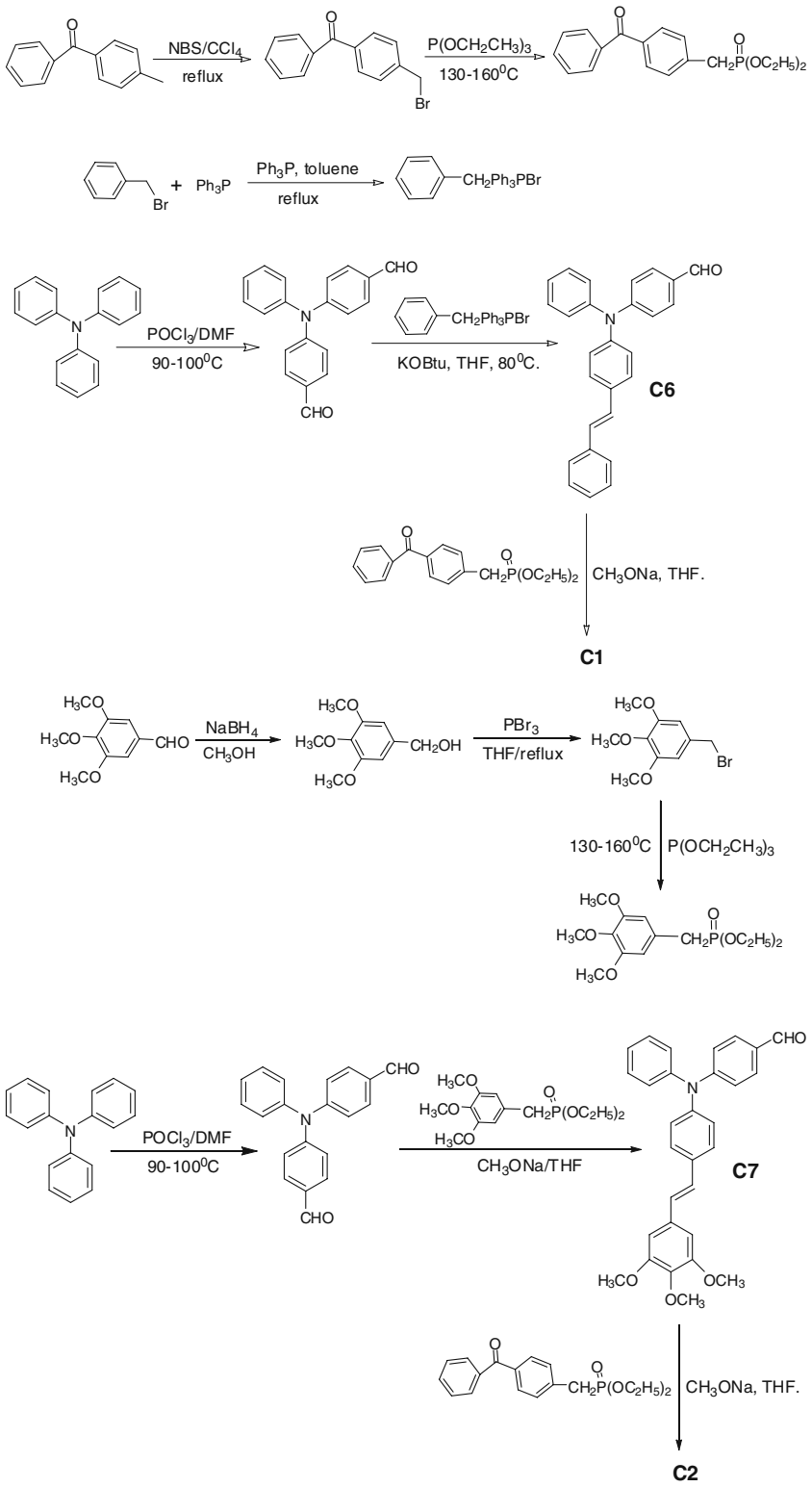

Scheme 1 (continued)

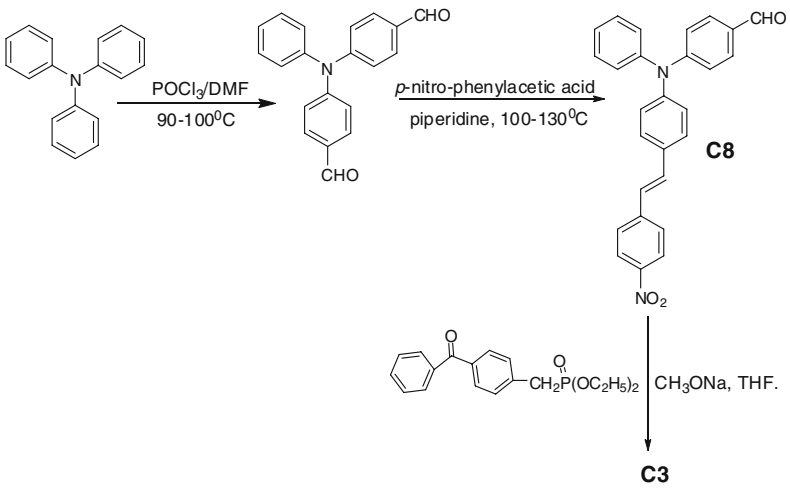

Electrochemistry

Electrochemical measurement was carried out using a Shanghai Chenhua working station. Two Pt work electrodes and an Ag/Ag^{+} reference electrode, namely three electrodes system, were included in a cell. Typically, a 0.05 mol/L solution of tetra-n-butylammonium hexaflorophosphate in methylene chloride containing of dyes was bubbled with argon for 15 min before the measurement.

Synthesis

4, 4′-Diformyl-triphenylamine was prepared according to well-known procedures with modified procedure. The synthesis of the derivatives was depicted in Scheme 1.

(1) 4-Bromomethylbenzophenone, which was prepared via bromide of 4-methylbenzophenone with N-bromosuccinimide [37], reacted with triethyl phosphate at 130–160 °C. After removed the excess triethyl phosphate under vacuum, the crude 4-phosphonate benzopheonone was obtained, which was used in the next step without further purification.

(2) Benzylbromidetriphenylphosphine salt was obtained from benzyl bromide and triphenylphosphine in toluene under reflux and purified with recrystallization in anhydrous ethanol.

(3) 3, 4, 5-Trimethoxyl-benzaldehyde was reduced with sodium borohydride in methyl alcohol. The reaction was preformed at room temperature under argon for 2 h. After the reaction, the solvent was removed in vacuum after the solid materials were filtered. The crude product was washed by water for five times. 3, 4, 5-Trimethoxyl-benzyl alcohol was purified with column chromatography using benzene as eluent. ^{1}H-NMR($CDCl_3$,500 MHz) δ (ppm): 6.42 (s, 2H, Ar-H), 5.10 (s, 1H, Ar-CH_2-*OH*), 4.52 (s, 2H, *CH_2*), 3.95 (s, 3H, Ar-*OCH_3*), 3.83 (s, 6H, Ar-*OCH_3*). Bromide of 3,4,5-trimethoxyl-benzyl alcohol was carried out in THF using phosphorus tribromide as bromine reagent under reflux. The solvent and excess phosphorus tribromide were removed in vacuum. The crude product was washed by distilled water for 5 times. 3, 4, 5-trimethoxyl-benzyl bromide was purified with recrystallization in benzene/cyclohexane (3:1). ^{1}H NMR ($CDCl_3$,500 MHz) δ (ppm): 6.35 (s, 2H, Ar-H), 4.10(s, 2H, *CH_2*), 3.77(s, 3H, Ar-*OCH_3*), 3.31(s, 6H, Ar-*OCH_3*)

5-Trimethoxyl-benzylbromide reacted with triethyl phosphate under 130–160 °C for 6 h. After excess triethyl phosphite was removed in vacuum, the crude 3′ 4′5-trimethoxyl-4-benzylphosphonate was obtained, which directly went to the next step without further purification.

(4) 4-Formyl-4′-(styrene)yl-triphenylamine (**C6**) was prepared from the reaction of benzylbromidetriphenylphosphine salt and 4,4′-diformyl-triphenylamine using

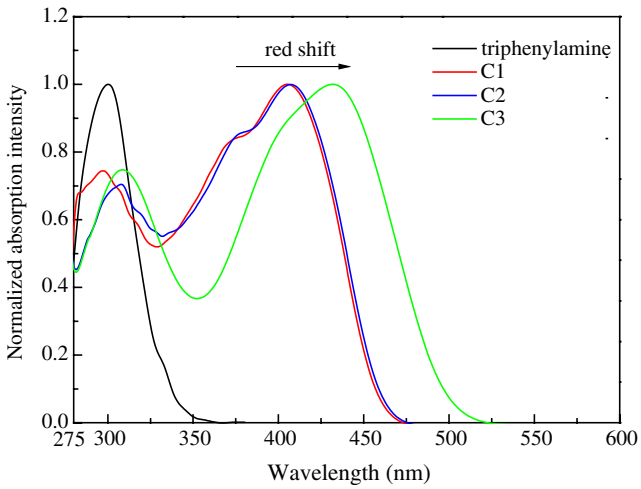

Fig. 2 UV/visible Normalized absorption spectroscopy of **C1**, **C2** and **C3** in benzene (*c*: 1×10^{-5} mol/L)

Table 1 Maximal absorption wavelength (λ_a: *nm*) and the molar extinction coefficients (ε) of the derivatives in various solvents

Compounds		Solvents				
		Benzene	THF	EtOAc	CH_2Cl_2	CH_3CN
C1	$10^{-5}\varepsilon$	0.397	0.437	0.463	0.438	0.394
	$\lambda_{a,max}$	406	405	407	410	404
C2	$10^{-5}\varepsilon$	0.440	0.498	0.512	0.494	0.522
	$\lambda_{a,max}$	406	406	407	411	404
C3	$10^{-5}\varepsilon$	0.416	0.484	0.504	0.462	0.516
	$\lambda_{a,max}$	432	431	431	432	427

ε $mol^{-1}\cdot l\cdot cm^{-1}$

tert-butoxide as base at room temperature. It was further purified with column chromophgraphy using benzene/ethyl acetate (*v*: *v*=4:1) mixed solvents as eluent and used in the next step. Yellow solid, yield: 40%, m.p.: 115–116 °C.^{1}H-NMR($CDCl_3$, 500 MHz) δ (ppm): 9.82(s, 1H, Ar-CHO), 7.680–7.707(d, 2H, J= 9.0 Hz, Ar-H), 7.513–7.515(d, 2H, J=7.5 Hz, Ar-H), 7.463–7.489 (d, 2H, J=9.0 Hz, Ar-H), 7.334–7.373(m, 4H, Ar-H), 7.245–7.260(t, 1H, Ar-H), 7.179–7.196(m, 3H, Ar-H), 7.146–7.177(d, 2H, J=8.5 Hz, Ar-CH= CH), 7.069–7.073(t, 4H, J=4.5 Hz, Ar-H). ^{13}C-NMR ($CDCl_3$,125 MHz):119.901, 125.267, 126.011, 126.368, 126.494, 127.688, 127.730, 127.744, 128.531, 128.749, 129.438, 129.818, 131.343, 134.042, 137.287, 145.536, 146.052, 153.117, 190.458.

(5) 4-(*p*-Benzoyl-styrene)yl-4′-(styrene)yl-triphenylamine (**C1**)

C1 was obtained from the reaction of 4-formyl-4′-(styrene)yl-triphenylamine (0.80 g, 2.13 mmol) and 4-benzylphosphonate benzopheonone (1.72 g, 3.20 mmol) in THF using sodium methoxide (0.35 g, 6.40 mmol) as base at room temperature. After the filtration of solid materials and the evaporation of THF in vacuum, the reactant mixture was dissolved in chloroform and washed by water. The organic layer was dried over magnesium sulphate. After evaporated in vacuum, **C1** was purified with column chromophg-raphy using benzene/petroether (*v*: *v*=5:1) mixed solvents as eluent. **C1**, yield: 58%, color, yellow, m.p., 126–127 °C, ^{1}H-NMR (d_6-benzene, 500 MHz, δppm): 7.781–7.829(m, 4H, Ar-H), 7.344–7.361(d,J= 8.5 Hz, 2H, Ar-H), 7.240–7.279(m, 6H, Ar-H), 7.193–7.223(t, J=7.5 Hz, 2H, Ar-H), 7.138–7.143(d, J= 2.5 Hz, 2H, Ar-CH=CH), 7.121–7.125(d, J=2.0 Hz, 2H, Ar-CH=CH), 7.085–7.110(m, 4H, Ar-H), 7.054–7.083(d, J=14.5 Hz, 2H, Ar-H), 7.008–7.041(t, J= 8.25 Hz, 2H, Ar-H), 6.989–7.000(t, J=2.75 Hz, 2H, Ar-H), 6.956(s, 1H, Ar-H), 6.891–6.911(m, 2H, Ar-H). ^{13}C-NMR(d-benzene,125 MHz):123.910, 124.001, 124.662, 125.309, 126.392, 126.419, 126.830, 127.675, 128.071, 128.294, 128.324, 128.398, 128.427, 128.943, 129.831, 130.163, 130.915, 130.957, 131.720, 131.991, 132.873, 136.734, 137.978, 138.653, 141.804, 147.311, 147.776, 148.119,195.120. Anal. Calcd for $C_{41}H_{31}NO$, C, 88.94, H, 5.64, N, 2.53, O, 2.89, Found, C, 88.87, H, 5.71, N, 2.59. IR (KBr) cm^{-1}: 3055.1, 3025.8, 2922.8 (=C–H), 1654.2(C=O), 1589.7, 1507.6(Ar-), 842.7 (*trans*-CH=CH-).

(6) 4-Formyl-4′-(3,4,5-trimethoxystyrene)yl-triphenylamine (**C7**) was firstly prepared from the reaction of 4-benzylphosphonate-(3,4,5-trimethoxybenzene) and 4,4′-diformyl-triphenylamine employing sodium meth-oxide as base at room temperature. It was purified with column chromophgraphy using benzene/ethyl acetate (*v*: *v*=45:1) mixed solvents as eluent and used in the next step. Yellow solid, yield: 50%, m.p.: 61–63 °C. ^{1}HNMR ($CDCl_3$,500 MHz) *δ*: 9.827 (s, 1H, Ar-C*H*O), 7.691–7.709 (d, 2H, J=8.5 Hz, Ar-H), 7.457–7.474 (d, 2H, J=8.5 Hz, Ar-H), 7.342–7.374 (t, 2H, J=8.0 Hz, Ar-H), 7.183–7.204 (m, 3H, Ar-H), 7.136–7.153 (d, 2H, J=8.0 Hz, Ar-C*H*=C*H*), 7.060–7.078 (d, 2H, J= 8.5 Hz, Ar-H), 6.986 (s, 2H, Ar-H), 6.735 (s, 2H, Ar-H), 3.92 (s, 6H, Ar-OCH_3), 3.87 (s, 3H, Ar-OCH_3). ^{13}C-NMR ($CDCl_3$, 125 MHz): 56.165, 60.990,

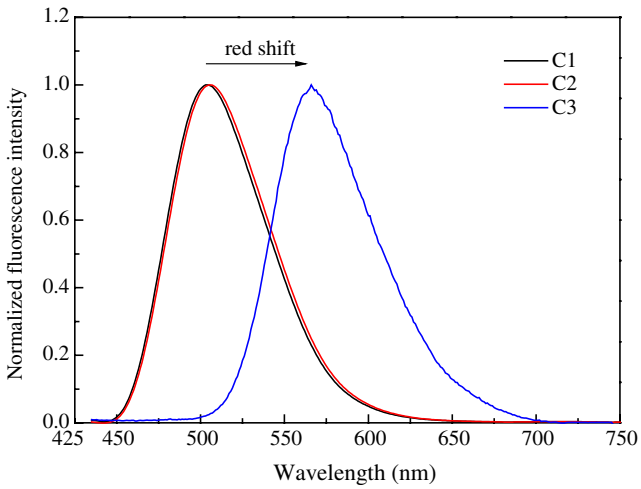

Fig. 3 Normalized fluorescence spectra of **C1**, **C2** and **C3** in benzene (*c*: 5×10^{-5} mol/L)

Table 2 Maximal fluorescence emission wavelength (λ_e: *nm*) and the fluorescence quantum yields (Φ) of the derivatives

Compounds		Solvents				
		Benzene	THF	EtOAc	CH_2Cl_2	CH_3CN
C1	ϕ	0.97	0.45	0.52	0.10	0.0034
	$\lambda_{f,max}$	493	535	527	549	541
C2	ϕ	0.93	0.23	0.29	0.029	0.0024
	$\lambda_{f,max}$	494	535	529	549	541
C3	ϕ	0.44	0.0055	0.0025		
	$\lambda_{f,max}$	542	596	590		

103.576, 119.922, 125.263, 125.981, 126.358, 127.193, 127.622, 128.419, 129.441, 129.805, 131.324, 133.022, 133.876, 145.509, 146.029, 153.099, 153.451, 190.449.

(7) 4-(*p*-Benzoyl-styrene)yl-4′-3,4,5-trimethoxyl-styrene) yl-triphenylamine (**C2**)

4-Formyl-4′-(3,4,5-trimethoxystyrene)yl-triphenylamine (1.20 g, 2.58 mmol) reacted with 4-benzylphosphonate benzopheonone (2.07 g, 3.87 mmol) using sodium methoxide (0.42 g, 7.74 mmol) as base at room temperature to prepare **C2**, which was purified with column chromophgraphy using benzene/ethyl acetate (*v*: *v*=45:1) mixed solvents as eluent. **C2**, yield: 65%, colour, orange, m.p., 80–82 °C. ^{1}H-NMR ($CDCl_3$,500 MHz, δppm):7.79–7.824(t, J=6.8 Hz,3H, Ar-H),7.713–7.728(d, J=7.5 Hz,1H, Ar-H), 7.575–7.591(d, J=8.0 Hz, 2H, Ar-H), 7.458–7.505 (t, J= 6.5 Hz, 2H, Ar-H), 7.360–7.444(m, 4H, Ar-H), 7.271–7.311(m, 2H, Ar-H),7.146–7.254(t, J=7.8 Hz, 3H, Ar-H), 7.001–7.130(m, 5H, Ar-H), 6.942–6.968(m, 2H, Ar-H), 6.718–6.729(d, J=12.6 Hz, 2H, Ar-CH = CH), 6.537–6.648(d, J=12.0 Hz, 2H, Ar-CH = CH), 3.917(s, 6H, OCH_3), 3.870(s, 3H, OCH_3). ^{13}C-NMR ($CDCl_3$,125 MHz):56.172, 61.017, 103.438, 123.591, 123.677, 124.242, 125.026, 125.889, 126.032, 127.399, 127.570, 127.927, 127.814, 128.305, 129.475, 129.952, 130.299, 130.832, 131.792, 132.042, 133.328, 135.972, 137.742, 137.947, 141.883, 146.846, 147.134, 147.696, 153.454, 196.101. Anal. Calcd for $C_{44}H_{37}NO_4$, C, 82.09, H, 5.79, N, 2.18, O, 9.94, Found, C, 81.99, H, 5.83, N, 2.11. IR (KBr) cm^{-1}: 3055.1, 3026.8, 2933.2(=C–H), 2833.6(−OCH_3), 1652.9(C = O), 1589.3, 1057.9(Ar-), 833.9(*trans*-CH = CH-).

(8) The crude 4-formyl-4′- (*p*-nitrostyrene)yl-triphenyl-amine (**C8**) was prepared from the reaction of *p*-nitro-phenylacetic acid with 4,4′-diformyl-triphenylamine at temperature of 100–130 °C (at 100 °C for 2 h, and then at 130 °C for 1 h till no production of CO_2). The compound was further purified with column chroma-tography with benzene/ethyl acetate (*v*: *v*=45:1) mixed solvents as eluent. Red solid, yield: 45%, m.p.: 172–173 °C. ^{1}HNMR($CDCl_3$, 500 MHz) *δ*: 9.84 (s, 1H, Ar-*CHO*), 8.21 (d, 2H, J=9.0 Hz, Ar-H), 7.72 (d, 2H, J= 9.0 Hz, Ar-H), 7.62 (d, 2H, J=9.0 Hz, Ar-H), 7.50 (d, 2H, J=8.5 Hz, Ar-H), 7.37 (t, 2H, J=6.8 Hz, Ar-H), 7.26 (d, 1H, J=3.0 Hz, Ar-*CH*= *CH*), 7.22 (d, 1H, 6.0 Hz, Ar-*CH*= *CH*), 7.17 (t, 5H, J=11.0 Hz, Ar-H), 7.10 (d, 2H, J=8.5 Hz, Ar-H). ^{13}C-NMR($CDCl_3$,125 MHz): 120.522, 124.198, 125.496, 125.529, 125.738, 126.525, 126.770, 128.314, 128.355, 129.866, 129.924, 131.334, 132.373, 132.410, 143.898, 145.925, 146.676, 146.781, 190.445.

(9) 4-(*p*-benzoyl-styrene)yl-4′-(*p*′-nitro-styrene)yl-triphe-nylamine (**C3**)

C3 was obtained from Wittig-Horner reaction of 4-benzylphosphonate benzopheonone (1.93 g, 3.61 mmol) and 4-formyl-4′-(p-nitrostyrene)yl-triphenylamine (1.00 g, 2.40 mmol) in THF (60 ml) using sodium methoxide (0.39 g, 7.21 mmol) as base at room temperature. After the filtration of solid materials and the evaporation of THF in vacuum, the reactant mixture was dissolved in chloroform and washed by water. The organic layer was dried over magnesium sulphate. After the evaporation of solvent in vacuum, **C3** was purified with column chromophgraphy using benzene/petroether (5:1) mixed solvents as eluent. **C3**, yield: 57%, color,

Table 3 Fluorescence lifetimes radiative transition constants and non-radiative transition constants of the derivatives

Compounds	Benzene			EtOAc		
	τ/ns	$Kr/_{10^7\,s^{-1}}$	$K_{nr}/_{10^7\,s^{-1}}$	τ/ns	$Kr/_{10^7\,s^{-1}}$	$K_{nr}/_{10^7\,s^{-1}}$
C1	2.039	47.57	1.470	2.248	23.130	21.350
C2	2.184	42.58	3.210	1.482	19.56	47.910
C3	3.055	14.40	18.330	–	–	–

τ: Fluorescence lifetimes (ns). K_r, radiative transition constants ($_{10^7\,s^{-1}}$) K_{nr}, non-radiative transition constants ($_{10^7\,s^{-1}}$)

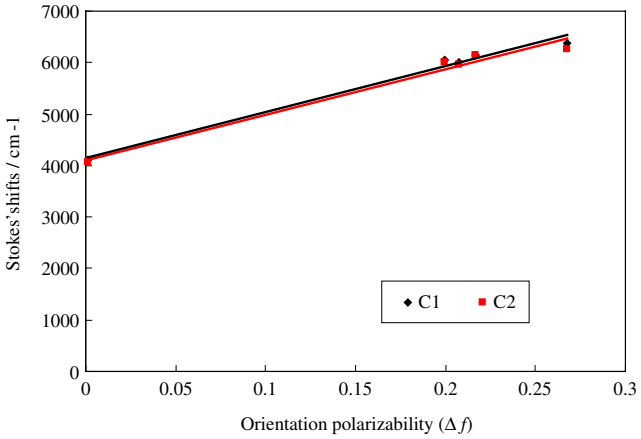

Fig. 4 Relationship between Stokes' shifts of the derivatives **C1** and **C2** and the orientation polarizability (Δf) of solvents respectively

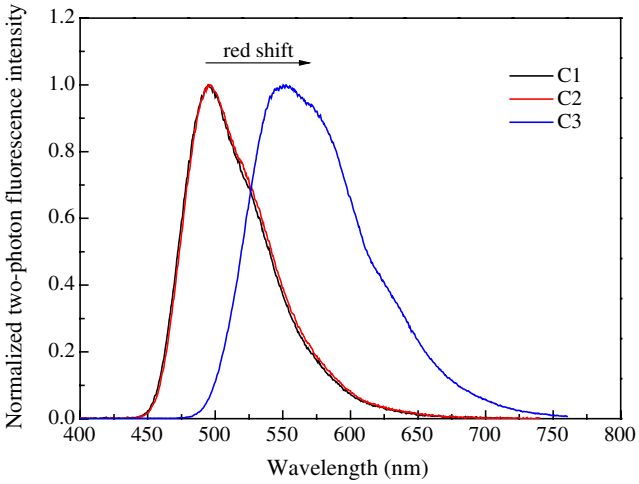

Fig. 5 Normalized TPA emission of the derivatives in benzene in 800 nm laser excitation (c: 5×10^{-4} mol/L)

red, m.p. 91-93 °C, ^{1}H-NMR($CDCl_3$, 500 MHz, δppm): 8.183–8.200(d, J=8.5 Hz, 2H, Ar-H), 7.795–7.820(t, J= 6.8 Hz, 4H, Ar-H), 7.575–7.589(d, J=7.0 Hz, 5H, Ar-H), 7.423–7.500(m, 6H, Ar-H), 7.295–7.325(t, J= 7.5 Hz, 2H, Ar-H), 7.216–7.243(t, J=6.75 Hz, 1H, Ar-CH=CH), 7.184–7.198(d, J=7.0 Hz, 1H, Ar- CH = CH), 7.147–7.163(d, J=8.0 Hz, 2H, Ar- CH = CH), 7.076–7.111(t, J=8.5 Hz, 6H, Ar-CH),7.006–7.040(d, J=17.0 Hz, 1H, Ar-H). ^{13}C-NMR($CDCl_3$, 125 MHz): 123.412, 124.057, 124.153, 124.546, 125.322, 126.025, 126.155, 126.531, 127.840, 128.064, 128.262, 128.320, 129.540, 129.900, 130.421, 130.659, 130.778, 131.527, 132.238, 132.695, 136.002, 137.859, 141.713, 144.462, 146.415, 146.816, 147.283, 148.006, 153.454, 196.000, Anal. Calcd for $C_{41}H_{30}N_2O_3$, C, 82.25, H, 5.05, N, 4.68, O, 8.02, Found, C, 82.17, H, 5.11, N, 4.62. IR (KBr) cm^{-1}: 3055.1, 3028.7, 2922.1(=C–H), 1650.4(C = O), 1628.0 (nitro-), 1583.9, 1507.6(Ar-), 842.0(*trans*-CH = CH-).

Results and Discussion

Synthesis

As shown in Scheme 1, conjugated double bonds in derivatives were constructed with different synthetic strategies. The branch without benzophenone part was attached to core firstly. For **C1**, this branch was constructed by Wittig reaction, and for **C2**, this branch was synthesized by Wittig-Horner reaction. While for **C3**, this branch was built by heating condensation. Owing to the electron-withdrawing effect of nitro group and the electron-donating of N core, the heating condensation reaction are able to occur between *p*-nitro-phenylacetic acid and 4,4′-diformyl-triphenylamine in weak base such as piperidine, and then C-C double bond is formed as carbon dioxide is produced. At the end, benzophenone part was coupled as the other branch of the derivatives by Wittig-Horner reaction. The target compounds could be purified easily through column chromophgraphy with the approximate 60% yield.

One-Photon Absorption and Emission Spectroscopy

Figure 2 shows that the derivatives exhibit double absorption peaks in 275–600 nm in benzene. The first absorption bands of the derivatives are similar to that of triphenylamine, which means that it may arise from the localized electronic transition of core. The absorption maxima of **C3** are larger than those of **C1** and **C2**, which could be ascribed to internal charge transfer character of (π, π^*) transition and **C3** has a larger intramolecular charge transfer [38]. Table 1

Table 4 Two-photon optical data of compounds **C1**, **C2** and **C3** in various solvents

Solvents	**C1**		**C2**		**C3**	
	λ_{max} (TPA)	σ_{TPA}/GM	λ_{max} (TPA)	σ_{TPA}/GM	λ_{max} (TPA)	σ_{TPA}/GM
Benzene	495	181	497	241	548	1,443
Ethyl acetate	544	147	544	142	640	1,687

λ_{max} *(TPA)* nm, the maximal up-conversion fluorescence wavelength; σ two-photon crossing section (GM, $1GM=10^{-50}$ cm·s·photo^{-1})

presents the linear absorption optical parameters in various solvents, including the maximal absorption and the molar extinction coefficients of the derivatives. The data show that the maximal absorption maxima of **C3** are approximate 30 nm red-shifted with respect to those of **C1** and **C2** in various solvents. Table 1 also shows that the derivatives have similar molar extinction coefficients because they have the same number of branches.

Figure 3 shows that the emission maxima of **C3** are red-shifted with respected to those of **C1** and **C2** in benzene. Table 2 lists the maximal emission wavelength and the fluorescence quantum yields of the derivatives. The emission of the derivatives exhibits more pronounced to solvent polarity than absorption, which results from larger intramolecular charge transfer in the excited states. As shown in Table 2, the maximal emission wavelength of **C3** is 40–60 nm longer than those of **C1** and **C2**, while **C1** and **C2** have much larger fluorescence quantum yields than **C3**, in various solvents. This could be ascribed to larger internal charge transfer and larger internal conversion in the excited state of **C3** due to electron-accepting effect of nitro group and the emission is thus prohibited.

The radiative transition constants and non-radiative transition constants of the derivatives are calculated according to the following equations:

$$Kr = \frac{\Phi_F}{\tau} \tag{4}$$

$$Knr = \frac{1 - \Phi_F}{\tau} \tag{5}$$

wherein $\boldsymbol{\Phi_F}$ is fluorescence quantum yield, τ represents as fluorescence lifetime, $\boldsymbol{K_r}$ is radiative transition constant, $\boldsymbol{K_{nr}}$ is non-radiative transition constant. Table 3 suggests that

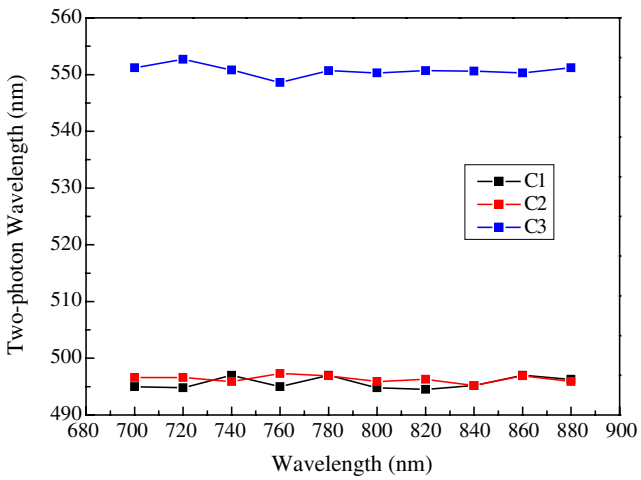

Fig. 6 Maximal TPA emission wavelengths of the derivatives in benzene excited by different laser wavelength

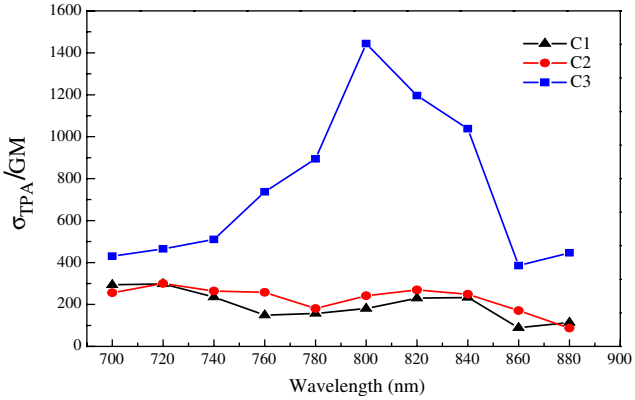

Fig. 7 TPA cross sections (σ_{TPA}) of **C1**, **C2** and **C3** in benzene in various laser wavelength (c: 5×10^{-4} mol/L)

C3 has larger non-radiative transition constants and smaller radiative transition constants, and **C1** and **C2** have similar radiative transition constants and non-radiative transition constants. This could explain why the emission of **C3** is

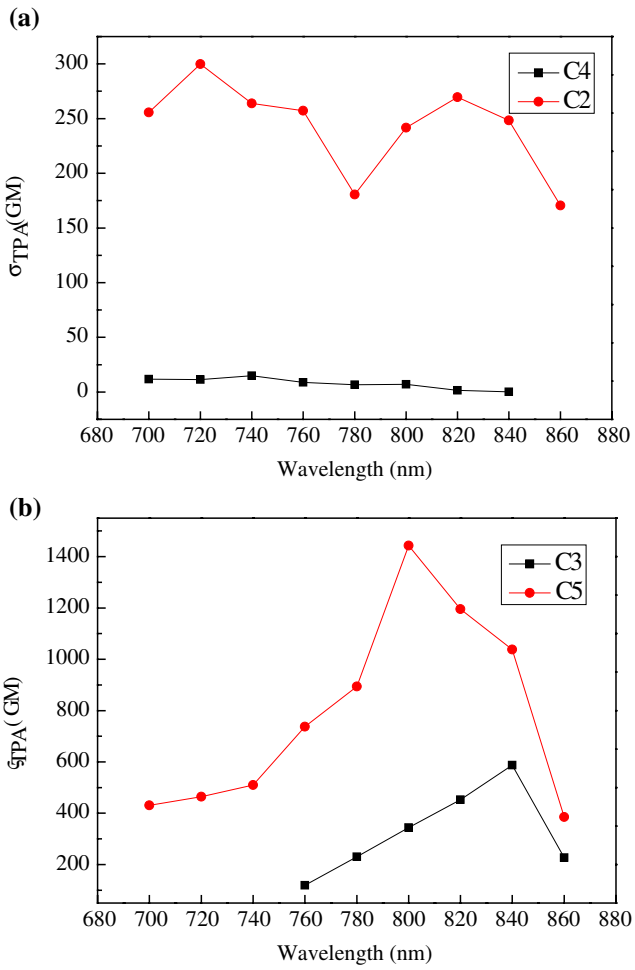

Fig. 8 Comparison of TPA cross sections (σ_{TPA}) of **C2**, **C3**, **C4** and **C5** in benzene in various laser frequencies (c: 5×10^{-4} mol/L) (**a**) HOMO and LUMO orbitals of the ground state (S_0) (**b**) HOMO and LUMO orbitals of the excited singlet state (S_1)

lower than those of **C1** and **C2**, and **C1** and **C2** have similar emission nature. We notice that the nonradiative transition constants of the derivatives are increased remarkably in polar solvents, which could be mainly ascribed to the enhancement of molecular geometric twist and extent of the internal charge transfer of (π, π*) transition, and accordingly nonradiative deactivation of the excited state is increased.

We have employed further Lippert equation to estimate the dipole moment changes of the derivatives as [39, 40]:

$$hc(\nu_{abs} - \nu_{em}) = \frac{2\left(\mu_e - \mu_g\right)^2}{4\pi\varepsilon_0 a^3}\Delta f + const \tag{6}$$

$$\Delta f = \left(\frac{\varepsilon - 1}{2\varepsilon + 1} - \frac{n^2 - 1}{2n^2 + 1}\right) \tag{7}$$

Wherein h represents as Planck's constant, c is the speed of light, and Δf is called the orientation polarizability. υ_{abs}, υ_{em} are the wavenumbers of the absorption and emission respectively, n is the refractive index, and ε is the relative low-frequency dielectric constant of the solvents. Lippert equation describes a solvent effect of the index of refraction and relative dielicetric constant. Because **C3** exhibit too weak photoluminescence in polar solvents, we did not perform Lippert equation for it. It is expected that **C1** and **C2** have similar dipole moment changes between the excited state and ground state.

Figure 4 plots the Stokes shift as a function of the solvent orientation polarizability (Δf) for the **C1** and **C2**. The linear correlations between Stokes shift and orientational polarizability indicates the dipolar solvent effects. The dipole moment changes between the excited state and the ground state are calculated from the slopes of lines:

$$\mathbf{C1}: Y = 8940.6X + 4141, \mathbf{C2}: Y = 8858.1X + 4105.1$$

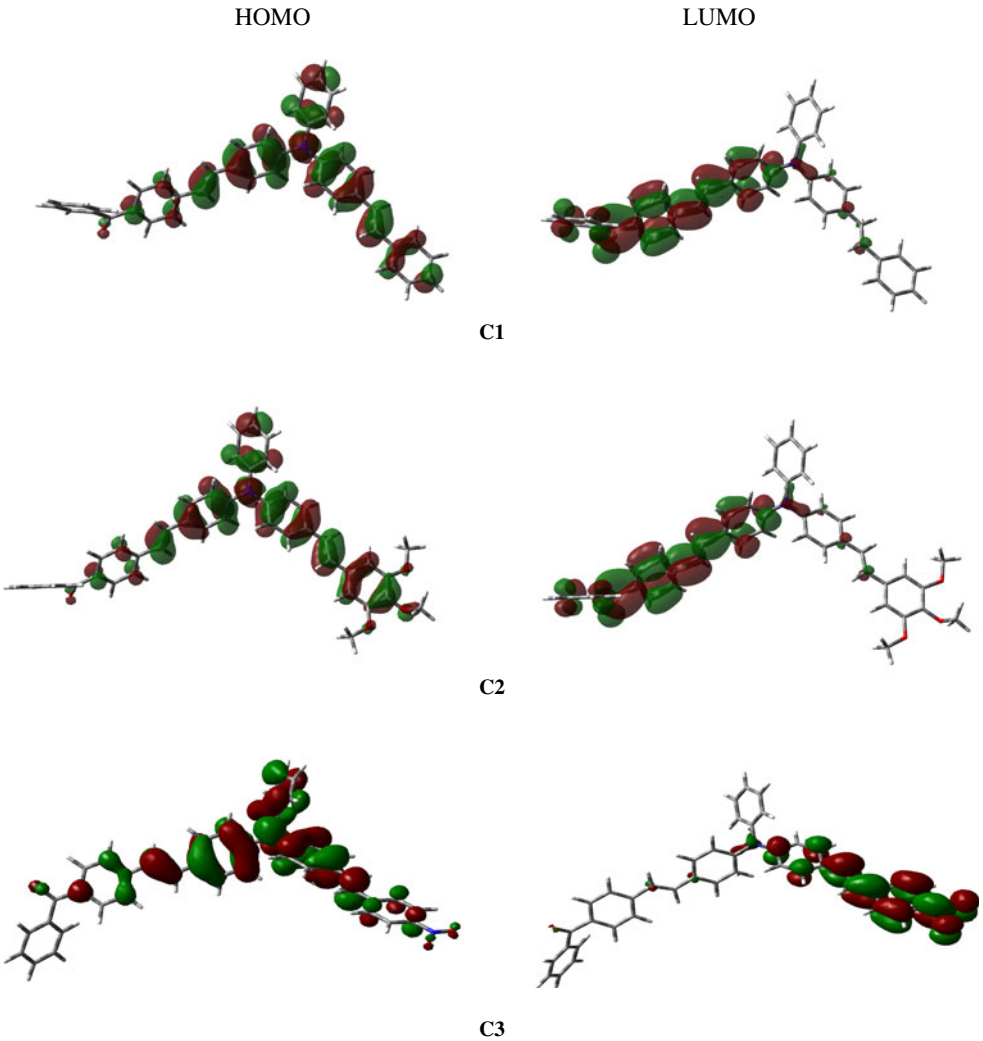

Fig. 9 Electron density distributions of frontier orbitals of **C1** **C2** and **C3** in the S_0 and S_1

(a) HOMO and LUMO orbitals of the ground state (S_0)

Fig. 9 (continued)

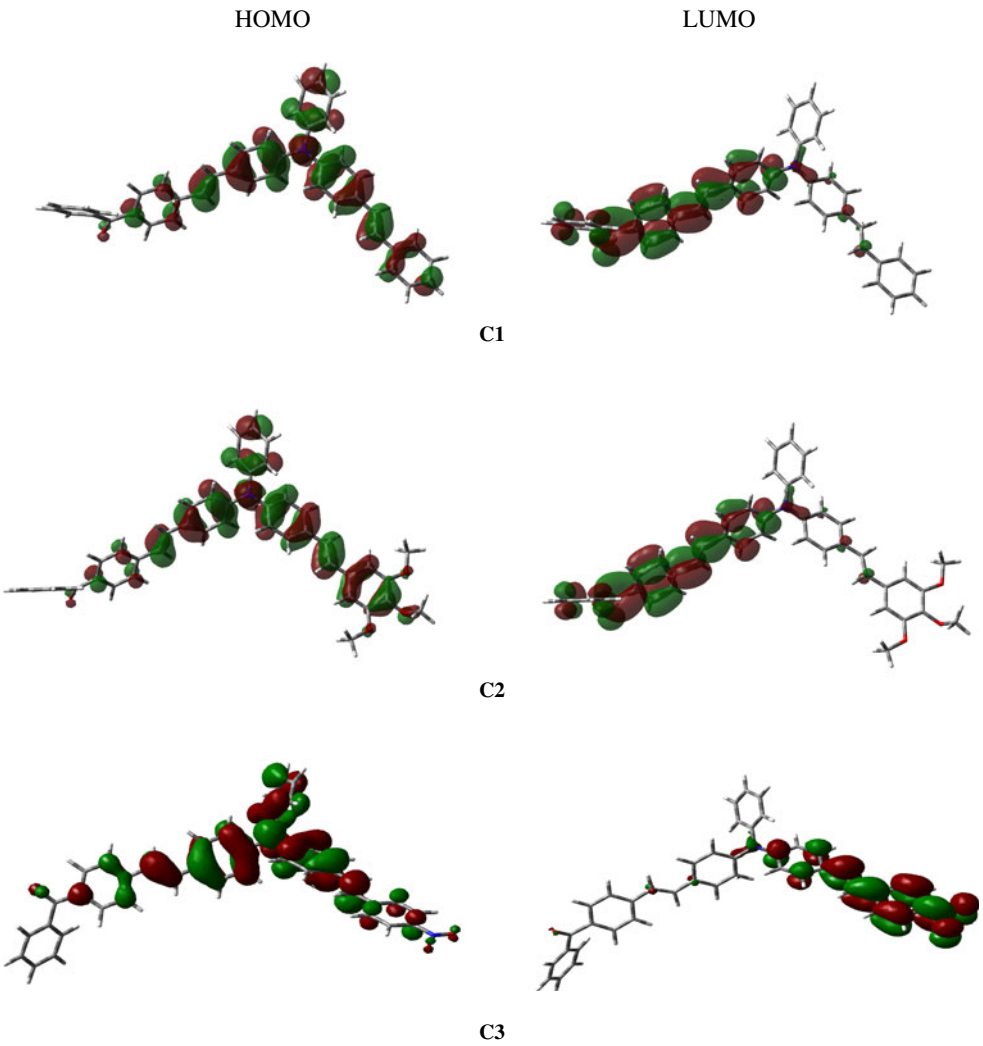

(a) HOMO and LUMO orbitals of the ground state (S_0)

The similar slopes from the lines imply similar solvent effects for the derivatives **C1** and **C2**, and close dipole moment changes are obtained as 6.00 and 6.48 Derby for **C1** and **C2** respectively, which could further account for the similar linear optical properties for **C1** and **C2**.

TPA Emission

Figure 5 presents that the maximal TPA emission wavelength of **C3** is red-shifted with respect to those of **C1** and **C2** in benzene. Seen from Table 4, **C3** has not only red-shifted TPA emission, but a larger cross section. We further determine TPA emission by tuning laser frequencies from 700 nm to 880 nm at intervals of 20 nm. It is interesting to observe that the maximal TPA emission of the derivatives is almost identical to one-photon emission wavelength and is almost irrelevant to that of excitation laser wavelength (Fig. 5), indicating the both emission could be from a similar excited state. TPA cross sections of **C3** are larger than those of **C1** and **C2** in benzene in various laser

Table 5 Energy gaps of HOMO and LUMO obtained from theoretical calculations in the ground state (S_0) and the excited state (S_1)

	C1		**C2**		**C3**	
	S_0	S_1	S_0	S_1	S_0	S_1
E_{HOMO}(ev)	−4.789	−4.951	−4.767	−4.919	−5.062	−5.177
E_{LUMO}(ev)	−2.047	−1.751	−2.035	−1.743	−2.446	−2.252
Energy gap (ev)	2.741	3.200	2.732	3.177	2.616	2.925

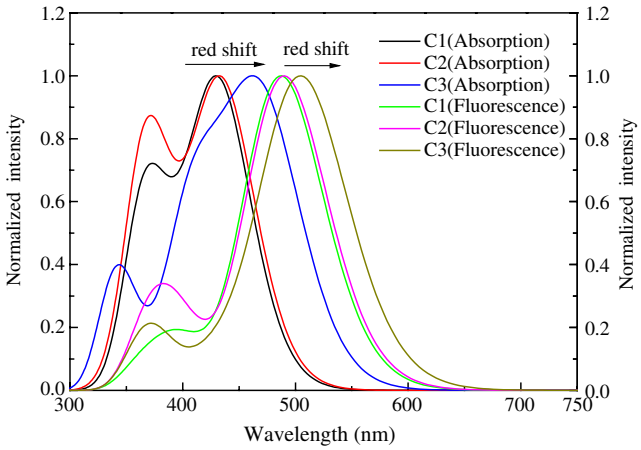

Fig. 10 Normalized calculated absorption spectra (obtained from TDDFT//HF), fluorescence spectra (obtained from TDDFT//CIS) of the derivatives

frequencies (Fig. 6), which could be due to larger dipole moment change of **C3** between the excited state and the ground state. The relationship of TPA intensities of the derivatives and the pumped powers follows well the square law in the excitation laser frequency 800 nm. The slopes of 1.98, 1.96 and 2.03 for **C1**, **C2** and **C3** respectively demonstrate that the derivatives have excellent two-photon absorption nature (Fig. 7).

Prasad and coauthors reported that two-photon cross section of **C3** was much larger than that of **C5** [41], indicating that benzophenone branch makes a contribution to TPA emission of the derivatives. We further prepared **C4** and **C5** and determined TPA cross sections of **C4** and **C5** under various near-IR Ti:sapphire femtosecond laser wavelength to compare. As shown in Fig. 8, TPA cross section of **C2** and **C3** are much larger than those of **C4** and **C5** under various near-IR laser wavelength excitation, which demonstartes that benzophenone branch has a significant effect on the enhancement of TPA emission of the derivatives containing benzophenone groups.

Molecular Geometry Optimization

The HOMO and LUMO orbitals in the ground and excite states were further analyzed. Figure 9 presents the electron density distribution of frontier orbitals of the derivatives. Obvious (π, π^*) transition with internal charge transfer occurs for the derivatives. In S_0 and S_1 states, the electron density distribution is mainly distributed around tripheylamine core in HOMO of the derivatives, and benzophenone branches of **C1** and **C2** have major electron contribution in LUMO orbital which confirms its donor-acceptor role. While for **C3,** the electron density contribution is mainly located in nitro branch of LUMO. Accordingly, **C1** and **C2** have similar electron density distribution, while it is

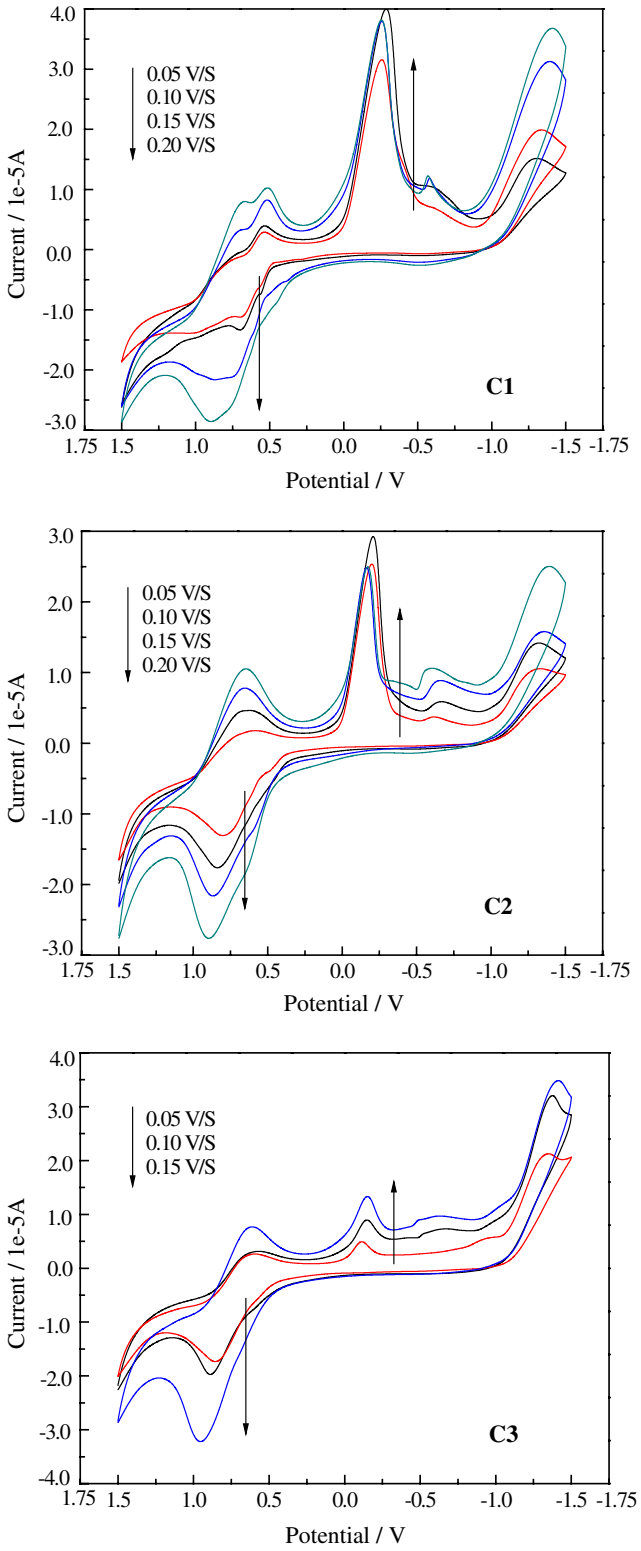

Fig. 11 Cyclic voltammetries of **C1, C2** and **C3** in methylene chloride at various scan rates

different from that of **C3**. We calculated dipole moment difference of the derivatives between the excited state and ground state. Remarkably, as our expectation, **C3** has a larger dipole moment change (2.33 D) than **C1** (1.43D) and **C2** (1.63D) in vacuum. Both experimental estimation and theoretical calculation demonstrate that **C1** and **C2** have similar dipole moment changes. Furthermore, HOMO-LUMO energy gaps in S_0 and S_1 of the derivatives were calculated and the results are shown in Table 5. **C3** has smaller HOMO-LUOMO energy gaps than **C1** and **C2** in both S_0 and S_1, while **C1** and **C2** have close HOMO-LUMO gaps. The above calculations well explains that the linear absorption, emission and TPA emission of **C3** is red-shifted and TPA cross section of **C3** is larger. The data also interpret why the derivatives **C1** and **C2** have similar linear and two-photon optical properties.

Figure 10 presents the calculated linear absorption spectra and fluorescence spectra of the derivatives, which were obtained with the Lorenz broadening of the anterior twenty excitation energies and corresponding oscillator strengths with Swizard program [42, 43] peak wavelength of the spectrum is equal to the corresponding singlet-singlet strongest transition energy. The values of absorption refer to the vertical transition from the S_0 states to the Franck-Condon S_1 states, while the value from the S_1 states to the corresponding Franck-Condon S_0 state yields an assignment to fluorescence [44]. The calculated absorption and emission maxima of **C3** are red-shifted with respect to those of **C1** and **C2**, and the derivatives **C1** and **C2** exhibit similar absorption and emission nature, which are well consistent with the experimental observation.

Cyclic Voltammograms

Figure 11 shows the cyclic voltammograms of the derivatives at the scan rates from 50 to 200 $mV{\cdot}s^{-1}$. No corresponding redox potentials demonstrate that redox processes of the derivatives dyes are characterized with irreversible nature under all sweeping rates. Furthermore, the linear increasing of peak currents with the square root of scan rates indicates that the redox processes of the derivatives are well dominated by the diffusion-controlled electron transfer reactions [49]. **C3** has a larger oxidation potential (0.889 V) than those of **C1** (0.701 V) and **C2** (0.832 V). On the other hand, the reductive peak potentials of **C3** (−0.501 V, −0.148 V) is much lower than those of **C1** (−0.285, 0.548 V) and **C2** (−0.208, 0.686 V). This could be ascribed to strong electron-withdrawing effect of nitro group, which could lower the reductive potentials, and increase oxidative potentials. We further estimated HOMO-LUMO energies from the optical band gap (E_g), which was calculated from the onset of the longest absorption wavelength at 10% of the maximal UV peak. Table 6 shows clearly that LUMO energy of **C3** is lower than those of **C1** and **C2**, but its HOMO is higher than those of **C1** and **C2**. As a consequence, **C3** has the lowest HOMO-LUMO gaps in these derivatives, which is in accordance with that of calculated result. This suggests that both HOMO and LUMO energies and HOMO-LUMO gaps of the derivatives could be affected by electro-withdrawing group.

Conclusions

This article presents some novel branched conjugated derivatives containing benzophenone group. One- and two- photon optical properties of the derivatives are much related to the chemical structures. We show strong evidences that benzopheonone branch does play significant role on the improvement of TPA nature of the derivatives carrying benzophenone moiety. Furthermore, the experimental and calculated results demonstrate that the electron density distribution, the energies and the energy gaps of the frontier orbitals of the derivatives are remarkably affected by electro-withdrawing substituent group, which results in large difference in internal charge transfer. These could be the deep reasons on the effect of substituent group on the optical properties of the derivatives. The results presented in this report would be of great interest in the development of new organic dyes carrying benzophenone moiety with ideal optical characteristics.

Table 6 Estimated HOMO and LUMO energies of the derivatives from redox potentials

Derivatives	λ_{onset}/nm	Gap/eV	E^{OX}	E_{LUMO}/eV	E_{HOMO}/eV
C1	460.0	2.70	0.70	−5.04	−7.74
C2	461.6	2.69	0.83	−5.17	−7.86
C3	503.2	2.46	0.89	−5.23	−7.69

E_g=1,240/λ, LUMO (*eV*)=- E^{OX} −4.34, [45, 46]. HOMO (*eV*)=LUMO - E_g, λ_{onset}:the longest absorption wavelength at 10% of the maximal UV peak [47, 48]

Acknowledgements The authors appreciate financial support from National Natural Science Foundation of China (Nos. 20776165, 20702065, 20872184). We would thank "the Foundation of Chongqing Science and Technology Commission" (CSTC2008BA4020, CSTC2009BB4216). H. Li thanks "A Foundation for the Author of National Excellent Doctoral Dissertation of PR China (200735)", and thanks the support from the Key Laboratory of Functional Crystals and Laser Technology, TIPC, Chinese Academy of Sciences. We also thank "Innovative Talent Training Project, the Third State of "211 Project, S-09103", Chongqing University.

References

1. Farruggia G, Iotti S, Prodi L, Montalti M, Zaccheroni N, Savage PB, Trapani V, Sale P, Wolf FI (2006) 8-Hydroxyquinoline derivatives as fluorescent sensors for magnesium in living cells. J Am Chem Soc 128(1):344–350
2. Sumalekshmy S, Henary MM, Siegel N, Lawson PV, Wu YG, Schmidt K, Brédas JL, Perry JW, Fahrni CJ (2007) Design of emission ratiometric metal-ion sensors with enhanced two-photon cross-section and brightness. J Am Chem Soc 129(39):11888–11889
3. Taki M, Wolford JL, O'Halloran TV (2004) Emission ratiometric imaging of intracellular zinc: design of a benzoxazole fluorescent sensor and its application in two-photon microscopy. J Am Chem Soc 126(3):712–713
4. Denk W, Strickler JH, Webb WW (1990) Two-photon laser scanning fluorescence microscopy. Science 248(4951):73–76
5. Picot A, D'Aléo A, Baldeck PL, Grichine A, Duperray A, Andraud C, Maury O (2008) Long-lived two-photon excited luminescence of water-soluble europium complex: applications in biological imaging using two-photon scanning microscopy. J Am Chem Soc 130(5):1532–1533
6. Tokar VP, Losytskyy MY, Ohulchanskyy TY, Kryvorotenko DV, Kovalska VB, Balanda AO, Dmytruk IM, Prokopets VM, Yarmoluk SM, Yashchuk VM (2010) Styryl dyes as two-photon excited fluorescent probes for DNA detection and two-photon laser scanning fluorescence microscopy of living cells. J Fluoresc 20(4):865–872
7. Chang CJ, Nolan EM, Jaworski J, Okamoto K, Hayashi Y, Sheng M, Lippard SJ (2004) ZP8, a neuronal zinc sensor with improved dynamic range; imaging zinc in hippocampal slices with two-photon microscopy. Inorg Chem 43(21):6774–6779
8. Claeyssens F, Hasan EA, Gaidukeviciute A, Achilleos DS, Ranella A, Reinhardt C, Ovsianikov A, Shizhou X, Fotakis C, Vamvakaki M, Chichkov BN, Farsari M (2009) Three-dimensional biodegradable structures fabricated by two-photon polymerization. Langmuir 25(5):3219–3223
9. Lee KS, Kim RH, Yang D, Park SH (2008) Advances in 3D Nano/Microfabrication using two-photon initiated polymerization. Prog Polym Sci 33(6):631–681
10. Sun W, Zhu H, Barron PM (2006) Binuclear cyclometalated Platinum(II) 4, 6-Diphenyl-2, 2′-bipyridine complexes: interesting photoluminescent and optical limiting materials. Chem Mater 18 (10):2602–2610
11. Vestberg R, Westlund R, Eriksson A, Lopes C, Carlsson M, Eliasson B, Glimsdal E, Lindgren M, Malmström E (2006) Dendron decorated Platinum(II) acetylides for optical power limiting. Macromolecules 39(6):2238–2246
12. Kim S, Ohulchanskyy TY, Pudavar HE, Pandey RK, Prasad PN (2007) Organically modified silica nanoparticles co-encapsulating photosensitizing drug and aggregation-enhanced two-photon absorbing fluorescent dye aggregates for two-photon photodynamic therapy. J Am Chem Soc 129(9):2669–2675
13. Belfield KD, Corredor CC, Morales AR, Dessources MA, Hernandez FE (2006) Synthesis and characterization of new fluorene-based singlet oxygen sensitizers. J Fluoresc 16(1):105–110
14. Karotki A, Khurana M, Lepock JR, Wilson BC (2006) Simultaneous two-photon excitation of photofrin in relation to photodynamic therapy. Photochem Photobiol 82(2):443–452
15. Pond SJK, Rumi M, Levin MD, Parker TC, Beljonne D, Day MW, Brédas J, Marder SR, Perry JW (2002) One- and two-photon spectroscopy of donor - acceptor - donor distyrylbenzene derivatives: effect of cyano substitution and distortion from planarity. J Phys Chem A 106(47):11470–11480
16. Rumi M, Ehrlich JE, Heikal AA, Perry JW, Barlow S, Hu Z, McCord-Maughon D, Parker TC, Röckel H, Thayumanavan S, Marder SR, Beljonne D, Brédas J (2000) Structure–Property relationships for two-photon absorbing chromophores: bis-donor diphenylpolyene and Bis(styryl)benzene derivatives. J Am Chem Soc 122(39):9500–9510
17. Lee S, Yang W, Choi JJ, Kim CH, Jeon SJ, Cho BR (2005) 2, 6-Bis[4-(p-dihexylaminostyryl)styryl]anthracene derivatives with large two-photon cross sections. Org Lett 7(2):323–326
18. Cho BR, Chajara K, Oh HJ, Son KH, Jeon SJ (2002) Synthesis and nonlinear optical properties of 1, 3, 5-Methoxy-2, 4, 6-tris (styryl)benzene derivatives. Org Lett 4(10):1703–1706
19. Mongin O, Porrès L, Moreaux L, Mertz J, Blanchard-Desce M (2002) Synthesis and photophysical properties of new conjugated fluorophores designed for two-photon-excited fluorescence. Org Lett 4(5):719–722
20. Pawlicki M, Collins HA, Denning RG, Anderson HL (2009) Two-photon absorption and the design of two-photon dyes. Angew Chem Int Ed 48(18):3244–3266
21. Bordeau G, Lartia R, Metge G, Fiorini-Debuisschert C, Charra F, Teulade-Fichou MP (2008) Trinaphthylamines as robust organic materials for two-photon-induced fluorescence. J Am Chem Soc 130(50):16836–16837
22. Fang Z, Teo TL, Cai LP, Lai YH, Samoc A, Samoc M (2009) Bridged triphenylamine-based dendrimers: tuning enhanced two-photon absorption performance with locked molecular planarity. Org Lett 11(1):1–4
23. Wei P, Bi XD, Wu Z, Xu Z (2005) Synthesis of triphenylamine-cored dendritic two-photon absorbing chromophores. Org Lett 7 (15):3199–3202
24. Chan EW, Chattopadhaya S, Panicker RC, Huang X, Yao SQ (2004) Developing photo-active affinity probes for proteomic profiling: hydroxamate-based probes for metalloproteases. J Am Chem Soc 126(44):14435–14446
25. Konry T, Novoa A, Shemer-Avni Y, Hanuka N, Cosnier S, Lepellec A, Marks RS (2005) Optical fiber immunosensor based on a Poly(pyrrole − benzophenone) film for the detection of antibodies to viral antigen. Anal Chem 77(6):1771–1779
26. Perrin D, Armarego W, Perrin D (1966) Purification of laboratory chemicals. Pergamon, New York
27. Gao F, Liu J, Yang L, Wang Q, Li H, Zhang S (2010) Chin J Chem 28(6):950–960
28. Fischer M, Georges J (1996) Fluorescence quantum yield of rhodamine 6G in ethanol as a function of concentration using thermal lens spectrometry. Chem Phys Lett 260(1–2):115–118
29. Maus M, Rettig W (1999) Photoinduced intramolecular charge transfer in a series of differently twisted donor-acceptor biphenyls as revealed by fluorescence. J Phys Chem A 103(18):3388–3401
30. Lukeman M, Veal D, Wan P, Ranjit V, Munasinghe N, Corrie JET (2004) Photogeneration of 1, 5-Naphthoquinone methides via excited-state (formal) intramolecular proton transfer (ESIPT) and photodehydration of 1-naphthol derivatives in aqueous solution. Can J Chem 82(2):240–253

31. Xu C, Webb WW (1996) Measurement of two-photon excitation cross sections of molecular fluorophores with data from 690 to 1050 nm. J Opt Soc Am B 13(3):481–491
32. Albota MA, Xu C, Webb WW (1998) Two-photon fluorescence excitation cross sections of biomolecular probes from 690 to 960 nm. Appl Opt 37(31):7352–7356
33. Zgiershi MZ, Grabowska A (2000) Photochromism of Salicylideneaniline (SA). How the photochromic transient is created: a theoretical approach. J Chem Phys 12(14):6329–6338
34. Yi PG, Liang YH, Cao CZ (2005) Intramolecular proton or hydrogen-atom transfer in the ground and excited-states of 2-hydroxybenzophenone: a theoretical study. Chem Phys 315 (3):297–302
35. Liang YH, Yi PG (2007) Theoretical studies on structure, energetic and intramolecular proton transfer of Alkannin. Chem Phys Lett 438(4–6):173–177
36. Yang ZN, Yang SY, Zhang JP (2007) Ground-and excited-state proton transfer and rotamerism in 2-(2-Hydroxyphenyl)-5-Phenyl-1, 3, 4-Oxadiazole and its O/″NH or S″-substituted derivatives. J Phys Chem A 111(28):6354–6360
37. Itoh T, Hall HK (1990) 7-Chloro-7-Phenyl-8, 8-Dicyanoquinodimethane. A novel initiator for cationic polymerizations. Macromolecules 23(22):4879–4881
38. Wang S, Kim SH (2009) Photophysical and electrochemical properties of D–π–A type solvatofluorchromic isophorone dye for pH molecular switch. Current Appl Phys 9(4):783–787
39. Lippert E (1957) Spektroskopische Bistimmung Des Dipolmomentes Aromatischer Verbindungen im Ersten Angeregten Singulettzustand. Z Electrochem 61:962
40. Lakowicz JR (1999) Principles of fluorescence spectroscopy. Kluwer Academic, New York
41. Lin TC, He GS, Prasad PN, Tan LS (2004) Degenerate nonlinear absorption and optical power limiting properties of asymmetrically substituted stilbenoid chromophores. J Mater Chem 14(6):982–991
42. Gaenko AV, Devarajan A, Tselinskii IV, Ryde U (2006) Structural and photoluminescence properties of excited state intramolecular proton transfer capable compounds-potential emissive and electron transport materials. J Phys Chem A 110(25):7935–7942
43. Gorelsky SI, Swizard program, revision XX, http://www.sg-chem.net/
44. Wang YL, Wu GS (2008) Electronic structure characteristics of ESIPT and TICT fluorescence emissions and calculations of emitting energies. Acta Phys Chim Sin 24(4):552–560
45. Liu J, Tu GL, Zhou QG, Cheng YX, Geng Y, Wang LX, Ma DG, Jing XB, Wang FS (2006) Highly efficient green light emitting polyfluorene incorporated with 4-Diphenylamino-1, 8-Naphthalimide as green dopant. J Mater Chem 16(15):1431–1438
46. Bard AJ, Faulkner LA (1984) Electrochemical methods-fundamentals and applications. Wiley, New York
47. Domagalska BW, Wilk KA, Wysocki S (2003) Experimental and theoretical studies on solvent effects of amphiphilic conjugated polyenals. Phys Chem Chem Phys 5(4):696–702
48. Ndaykengurukiye H, Jacobs S, Tachelet W, Looy JVD, Pollars A, Geise HJ, Claeys M, Kauffmann JM, Janietz S (1997) Alkoxylated p-Phenylenevinylene oligomers: synthesis and spectroscopic and electrochemical properties. Tetrahedron 53(40):13811
49. Aoki K, Guo Y, Chen JY (2009) Diffusion-controlled currents in viscous solutions of polyethylene glycols. J Electroanal Chem 629 (1–2):73–77